International Conference on Space Optics—ICSO 2014

La Caleta, Tenerife, Canary Islands

7–10 October 2014

Edited by Zoran Sodnik, Bruno Cugny, and Nikos Karafolas

HgCdTe APDS for space applications

Johan Rothman

Eric de Broniol

Kevin Foubert

Laurent Mollard

et al.

HGCDTE APDS FOR SPACE APPLICATIONS

Johan Rothman [1], Eric de Broniol[1], Kevin Foubert [1], Laurent Mollard[1], Nicolas Péré-Laperne[2], Frederic Salvetti[2], Alexandre Kerlain[2], Yann Reibel[2]

CEA/Leti, Minatec Campus, 17 rue des Martyrs, 38054 Grenoble Cedex, France :
johan.rothman@cea.fr , [2] Sofradir, BP 21- 38113 Veurey-Voroize- FRANCE

Abstract— **HgCdTe avalanche photodiode focal plane arrays (FPAs) and single element detectors have been developed for a large scope of photon starved applications. The present communication present the characteristics of our most recent detector developments that opens the horizon for low infrared (IR) photon number detection with high information conservation for imaging, atmospheric lidar and free space telecommunications. In particular, we report on the performance of TEC cooled large area detectors with sensitive diameters ranging from 30- 200 µm, characterised by detector gains of 2- 20 V/µW and noise equivalent input power of 0.1-1 nW for bandwidths ranging from 20 to 400 MHz.**

Keywords- APD, HgCdTe, focal plane array, LIDAR, free-space telecom, LADEE, LLCD

I. INTRODUCTION

HgCdTe have been shown to exhibit close to optimal amplification properties characterised by an exponential increasing linear gain as a function of reverse bias, up to multiplication factors higher than 1000, close to negligible excess noise and a response time which is close to independent of gain. These characteristics have opened new perspectives in most fields of low photon number detection at wavelengths reaching from the uv to the Infra-Red (IR) detector cut-of wavelength. The high performance of HgCdTe APDs is principally due to multiplication through impact ionisation which is exclusively initiated by the electrons. For this reason, theses APDs have been termed electron initiated APDs (e-APDs) or single carrier multiplication APDs (SCM-APDs).

At present, an increasing number of groups [1]-[6] have confirmed the close to constant exponential increase of the gain as a function of reverse bias up to values larger than 1000, associated with a close to constant signal to noise ratio (SNR). Such performances have been demonstrated in HgCdTe APDs with x_{Cd} lower than 0.5. The HgCdTe APDs do also have low dark currents at high gains [7], [8] and a response time which is close to independent of the gain [9]-[12]. The latter is again related to exclusive electron multiplication, which guarantees that the response time is limited by a single transit time of the depletion region width for each type of carrier [9]-[12]. The experimental and numerical studies of the carrier dynamics during the multiplication suggests that bandwidths in the range of 10-30 GHz should be achievable in HgCdTe APDs at gains higher than 100, although the highest bandwidth so far is in the range of 600 MHz to 1 GHz [10, 12].

These characteristics are complemented by a high gain homogeneity which makes HgCdTe APDs suitable for imagery application. Consequently, high performance focal plane arrays have been developed for active [2,6,7,13-17] and passive imaging [14,18]. Four HgCdTe APD FPAs have been developed at CEA/Leti and Sofradir so far [15-18]. The main characteristics of these FPAs and the perspectives for using the APD FPAs for space applications will be presented in section III, after the presentation of the typical performance that is currently obtained with HgCdTe APDs as a function of x_{Cd} composition (section II). HgCdTe APd can also be used for single pixel application in which the temporal information/variation of the light is detected. The more recent development of such single element HgCdTe APD detectors for LIDAR, free-space optical telecommunications (FSO) and laser range finder is presented in section IV. The results obtained with the HgCdTe APD detectors and the perspectives for space applications are resumed in section V.

II. HGCDTE APDs CHARACTERISTICS

The HgCdTe APDs made at Leti and Sofradir are manufactured using liquid phase epitaxial grown epi-layers with close to constant Cd composition. A homo-junction with a large n- region is formed by the n-type conversion of a spatially localized region close to the device surface.

High performance HgCdTe e-APDs have been developed with cut-off wavelengths (λ_c) ranging from 2.5 to 5.6 µm by adjusting the Cd composition in the absorption and multiplication region. Gain curves measured at T=80 K for APDs with various λ_c are compared in Fig. 1. Typical performances of SWIR and MWIR APDs at T=80 K are compared in Tab. 1. It can be seen that the gain decreases with λ_c. The variation in gain is mainly due to the increase of the bandgap. The maximum gain in Tab. 1 corresponds to the highest stable gain values and ranges from 2000 for SWIR APDs to higher than 10 000 in MWIR APDs. The usefulness of such high gains depends on the dark-current noise of the APD, the observation time and the noise of the detection

electronics. Stable gain, associated with low noise, has been observed up to room temperature in SWIR APDs [19]. The usefulness of this characteristic depends again on the acceptable dark current noise which is function of the amplifier noise and the bandwidth in each application.
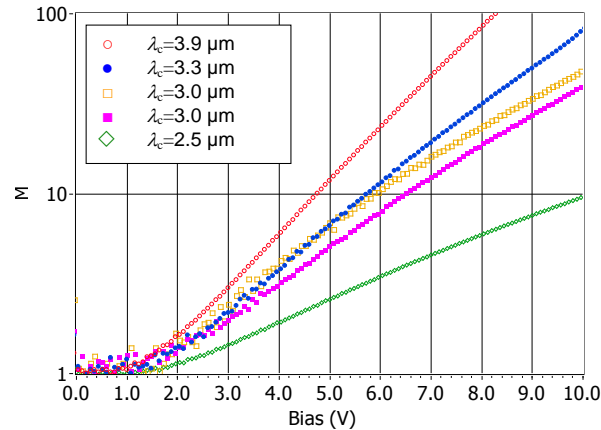
Fig. 1. Gain curves estimated in HgCdTe APDs with cut-off wavelengths λ_c=2.5-3.9 µm at 80K.

Low F values, F=1.1-1.4, associated with high quantum efficiencies (QE) yields a QE to F ratios (QEFR) >50 % for all λ_c. QEFR measures the conservation of the information contained in a shot noise limited photon flux in linear amplified photo-detectors. The QEFR values observed for HgCdTe APDs are the highest values reported for any amplified linear photodetector so far. The conservation of this property for all x_{Cd} allows choosing the Cd composition of the device for each application as a function of system requirements, such as the characteristic time of observation (TC), number of photons per TC, amplifier noise and acceptable dark current noise. The dark current and noise tends to decrease with decreasing λ_c at constant gain and temperature [15]. This implies that low operating temperature and low λ_c is required for low flux applications with long TC. The lowest observed equivalent dark noise currents of 12 e/s has been measured in λ_c=2.9 µm APDs at a gain of 24 at T=80 K, which limits the maximum integration time to about 1 s for an equivalent read-out noise of 3-4 electrons. Lower dark currents and noise is expected for lower λ_c, gain and operating temperature. For fast observations with short observation times, TC<1µs, the operating temperature and/or cut-off wavelength can be increased. In particular, HgCdTe APDs with λ_c =3.0 µm at 300K can be used in applications with GHz bandwidth. As can be seen in Tab. 1, such high bandwidths has not yet been achieved in HgCdTe APDs due to slow carrier collection through diffusion and/or impedance mismatch (BW=40-600 MHz). Impulse response-time measurements have however shown that bandwidths of 10 to 20 GHz should be achievable in SWIR and MWIR APDs designed for fast response [10, 12].

Parameter	SWIR	MWIR
Quantum efficiency	60-80 %	
Max gain	2 000	13 000
Bias at M=100	12-14 V	7-10 V
Excess noise factir F	1.1-1.4	
QEFR	40-70 %	
I eq_in at M=100	2 aA	10 fA
Typical response time T90-10	0.5-20 ns	
Maximum GainxBW product	2.1 THz	

Tab. 1. Typical performance of SWIR and MWIR HgCdTe APDs at T= 80 K

III. PERSPECTIVES FOR HGCDTE APDS FPAS FOR SPACE APPLICATIONS

The development of HgCdTe APD FPAs has principally been motivated by ground based applications. The Tab. 2 describes the characteristics of the APD FPAs that have been developed so far by CEA-Leti and Sofradir [15-19]. The main development has been dedicated to active imaging. The most interesting active-imaging FPA for space application at present is the large format real-time 3D imager, which can be used for automatic localization during the approach to planets and for obstacle avoidance during landing of space vehicles. The temporal resolution of this FPA was 1-2 ns in the time of flight (TOF) for a signal of 100 photons per pixel, corresponding to a distance between 15 and 30 cm. This first demonstrator was not dedicated to 3D imaging and we expect to obtain a similar resolution in distance for down to 5 to 10 photons per pixel.

One dedicated APD FPA has been developed for passive imaging. This FPA was designed for earth base wavefront correction and interferometry using fast frame rate imaging with frame rates up to 1500 fps with a minimal read-out noise. These FPAs have a high operability in terms response and average read-out noise below 2 electrons for a maximum APD gain of 20. However, at longer integration time, the glow from the

Imaging modes	Applications	Format	APD arrays	Frame rate	Top performance
Passive and active (range gated)	Thermal imaging, long range identification, de-camouflage	320x256, 30 µm pitch	λc=2.5-5 µm, M=1 100, operability >99 %, σ/M<5%, F=1.1-1.4, Top=80-200 K	450 Hz	100 ns gate, min Ieq_in=2aA, 90/M electrons nosie rms
Passive,active and 3D (time of flight)	Thermal imaging, long range identification, aerospatial navigation,de-camouflage	320x256, 30 µm pitch		60 Hz	1ns single shot range noise
Passive and active (range gated)	Thermal imaging, long range identification, de-camouflage	380x288, 15 µm pitch		200 Hz	35 ns gate, rise/fall time <5 ns
Passive high frame rate, multi parametric	Wavefront correction, fringe tracking, hyper-spectral imaging	320x256, 30 µm pitch		1500 Hz	30/M electrons noise rms/frame

Tab. 2. Typical performance of MWIR HgCdTd APDs

readout circuit is detected by the APDs. This limits the maximum integration time to about 100 ms, considering a gain of 10 to 30 as observed in the present generation of FPAs [19]. Hence, the use of the RAPID FPA is limited to applications with sub second integration times. For lower flux applications, a lower glow read-out circuit must be used. Such a circuit has been designed at CEA/Leti using a source follower to probe the charge integrated on the APD [20] with a format of 640x512 and a pitch of 15 µm. This hybridization of this ROIC, which is characterized by a read-out noise below 10 electrons using correlated double sampling read-out, with APD arrays opens the perspective of sub electron rms read-out noise for integration times up to 10 seconds.

IV. SINGLE ELEMENT HGCDTE APDs DETECTORS

Single element HgCdTe APD detectors have been developed to address the large number of applications that do only need to recover the temporal information carried by the optical signal in one single channel. This is the case in LIDAR and optical data transfer applications. The development of single element APD detectors could seem straight forward once large area FPA have been realized with high operability. This extrapolation is particularly true concerning the yield of fabrication of large area detectors. However, the detector size, packaging and proximity electronics need to be adapted to each application in order to obtain optimized performances. At present, we have developed four prototype detectors for LIDAR, free space optical telecommunication, near infrared spectroscopy and photon counting. The performance obtained for slow spectroscopy measurements has been reported previously in reference [21] and the present communication is dedicated to detectors for atmospheric LIDAR, free space optical telecommunication (FSO) and eye-safe laser range finders, described in sub-sections A and B, and to the perspective of single photon detection, reported in sub-section C.

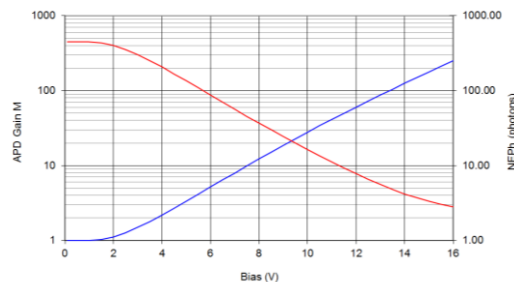*A. Development of large area single element HgCdTe APDs for LIDAR and FSO*

Fig. 2. Estimation of the gain and the sensitivity (*NEPh* per *TC*) of a 100 µm diameter HgCdTe APD with λ_c=3.1 µm operated at T=190 K in coupling with a TIA with an input noise of i_{TIA}=2 pA/Hz and a *BW* of 300 MHz.

The required temporal resolution in most LIDAR and FSO applications ranges between 50 ns to 250 ps, corresponding to bandwidths between 100 MHz and 2 GHz. The active optical diameter dependence on the receiver optics and is typically in range of 80 to 200 µm. These specifications define the parameter space in terms of Cd composition as a function of system requirements such as operating temperature, sensitivity and active area. The sensitivity is ultimately limited by the dark noise of the APD, induced by the dark current and residual thermal flux, which should be lower than the input referred noise of the pre-amplifier. In the present development, we have chosen to work with detectors cooled down to temperatures around 200 K. This allows using thermo-electric cooling (TEC), in ground based applications, or passive cooling, in space applications. In order to obtain the lowest possible temperature and largest optical active area, we have chosen to deport the amplifier off the cold-down surface rather than to hybridize the APD on the amplifier. This choice implies a higher amplifier noise which needs to be overcome by a higher APD gain. In addition to guarantee a lower detector noise, due to lower APD dark noise, this choice is also more versatile as it allows changing the APD λ_c and surface with a given amplifier and/or the amplifier with a given APD as a function of application requirements. Higher sensitivities, down to single photon sensitivity, can be obtained at lower temperatures

using application hybridized read-out circuits. The development and perspectives for such detectors are described in sub-section C.

A model have been developed to predict the performance of such HgCdTe APDs coupled with a pre-amplifier with a given noise and bandwidth. The gain of the APD as a function of x_{Cd} and operating temperature based on an analytical gain model we presented in reference [22]. The dark current noise and noise is calculated supposing a diffusion current generation at all temperatures, which is multiplied with the total gain of the APD. The sensitivity of the detector is measured as the equivalent photon number noise, NEPh, integrated during the characteristic time of the amplifier $TC=1/2BW$.

$$NEPh = \frac{hc}{\lambda} \frac{I_n TC}{QE}$$

(1)

where I_n is the input referred rms noise current:

$$I_n = \sqrt{\left[\left(\frac{i_{TIA}}{M}\right)^2 + 2qFI_{dark}\right] xBW}$$

(2)

The Fig. 2 shows the calculated gain and NEPh of a single element detector as a function of the reverse bias for a 100 µm diameter APD with $x_{Cd}=0.37$ operated at $T=190$ K ($\lambda_c=3.1$ µm), coupled with a preamplifier with a bandwidth of 300 MHz and an input referred noise $i_{TIA}=2$ pA/√Hz. The sensitivity approaches single photon resolution with $NEPh=2.87$ photons per TC, corresponding to a noise equivalent power (NEP) of less than 300 pW. This is 10 better than the highest performance reported for InGaAs APDs receiver with equivalent size and lower bandwidth, NEP=3 nW at $BW=100$ MHz [23]. Photon resolution can however not be achieved at this operating temperature due to the dark current noise of the APD which is the origin of the saturation of the NEPh reduction observed at high reverse bias.
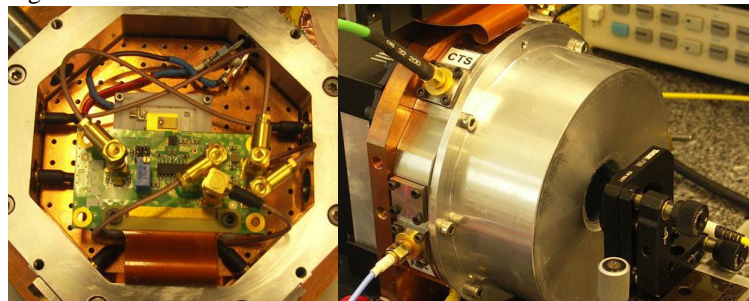

Fig. 3. Photography of a) the inside of a HgCdTe APD detector module and b) of a closed detector assembly.
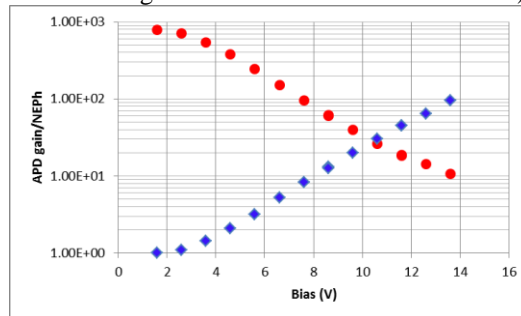

Fig 4. Variation of the detector gain and input equivalent photon noise of the detector module used during the lunar laser communication demonstration at ESAs OGS at Tenerife.

Two large area TEC cooled detector modules with deported TIA have been developed using TIAs with bandwidth and noise adapted for FSO (BW=400 MHz, $i_{TIA}=2$ pA/) and LIDAR (BW=20 MHz, $i_{TIA}=1$ pA/Hz). The detector assembly with the high BW TIA is illustrated in Fig. 3. The performance of the two detector modules are compared in Tab. 3. The measurements on the detector APD3-TIA-1 were made by imaging the output of a 200 µm diameter multi-mode fibre on to the APD. Hence, the characterisation of the total detector gain (3 MV/W) and estimated quantum efficiency (58 %) include losses due to the optical coupling from the fibre to the detector. The measured variation of the signal gain and NEPh is reported in Fig. 4. The output noise at the nominal gain was slightly higher than the amplifier noise, mainly due to the detection of residual thermal

| Parameter	APD3_TIA-1	APD1-TIA-2
BW TIA/APD (MHz)	350/80 (220)	20/NA
λ_c (µm)	3.14	2.9
$\phi_{detector}$ (µm)	160	200
Bias (V)	14.8	16
Gain (MV/W)	3.0	23
External QE (%)	58	67
APD Gain	95	80
Output Noise (mV)	2.2	3.1
NEP (nW)	0.73	0.13
NEP (fW/√Hz)	42	30.1
NEPh/TC (photons)	9.1	30

Tab 3. Performances of the high and low bandwidth detectors.

photon flux which needs to be limited by, for example, adding cold optical filters. A record low *NEP* =0.73 nW for this level of bandwidth was still observed, which is a factor 4 lower than the values observed in InGaAs APDs for detectors with a factor 4 lower TIA bandwidth. The corresponding rms input noise is about 9 photons per *TC*, which is comparable to the predictions in Fig 2. The bandwidth of the detector module were limited the diffusion collection of photo-generated carriers before avalanche multiplication, *BW*=80 MHz. The impulse response time of detector is illustrated in Fig. 5. This detector module has been used to demonstrate error free data transmission from the moon to ESAs OGS telescope at Tenerife at rate of 80 Mbit/s. The results of these measurements are presented in the next section.

The slower detector module was build using TIA-2. This TIA is DC coupled and the total gain can be measured using a CW laser light (λ =1.55 µm). The total detector gain of *S*=294 kV/W was measured at unity APD gain, which corresponds to an external quantum efficiency of 67 %. At 16 V bias, the apparent APD gain is 80 and the total detector gain reaches a value of 23 MV/W. The linearity of the detector was tested at an APD gain of 23. The detector was found to have a good linearity of more than 3 orders of magnitudes, as illustrated in Fig. 6. The output noise of the TIA was higher than expected even at low reverse bias. The increase in noise is probably induced by parasitic impedances at the input of the amplifier. At higher bias we observed a slight increase in noise, again due to residual thermal photons. The corresponding *NEP* at a gain of 80 of this slower detector module is 0.13 nW (30 fW/√Hz). High detector gain and lower noise can be expected in detectors with lower TIA noise and higher APD gain with NEP values lower than 20 fW/√Hz. An optimized version of this detector will be transferred to Laboratoire de Metrologie Dynamique (LMD) to be used for Differential absorption LIDAR (DIAL) detection of atmospheric CO_2, in the scope of a CNES R& T project. Similar detector elements will also be subject to first space reliability tests on APDs made at CEA/Leti.
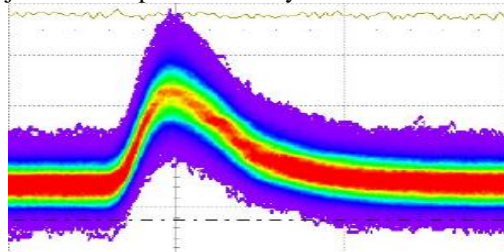
Fig 5. Impulse response of a 160 µm diameter APD coupled with TIA-1, operated at T=190 K with a gain of M=95 to an impulse of 100 photons. The vertical and horizontal scales are 5 ns and 10 mV per division, respectively.
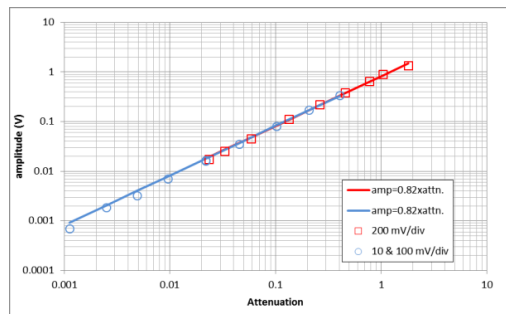
Fig 6. Pulse amplitude linearity measured on a 200 µm diameter HgCdTe APD coupled with TIA-2 at *T*=180 K with and APD gain M=23.

B. Demonstration of lunar optical communication link (LOCL) with HgCdTe APD during the LLCD-LADEE mission
The APD3-TIA-1 detector module have been used during the demonstration of a laser optical communication down link from the moon, as a part of ESAs contribution to the Lunar Laser Communication Demonstration (LLCD) with the LADEE satellite orbiting around the moon. In this demonstration, the data was encoded using 16ary pulse position modulation (PPM) with pulse durations from 3.2 ns (Mode 5, decoded transmission rate of 39 Mbits/s) down to 0.2 ns (Mode 1, decoded transmission rate of 625 Mbits/s). The expected average power on the detector has been predicted to be around 300 pW, corresponding to about 120 photons per pulse during Mode 5 modulation, i.e. close to the average photon number of the impulses in Fig. 5.
The performance of the APD detector module was first tested as a function of input average power using laboratory generated Mode 5 and Mode 4 modulated light. The detector output signal was decoded using an electron unit developed at RUAG as described in [24]. Fig. 7 a) and b) report the variation of the symbol and decoded frame error rate as a function of the average power at the output of the optical power. The error rate was estimated over a test pattern with 10^5 bits, which enable the estimation of frame error rates down to 10^{-5}. To this limit error free detection was achieved for average optical power down to 20 photons per decoded bit,

corresponding to 40 photons per impulse and 100 pW average power, in mode 5 (Fig. 7 a)). Due to the bandwidth limitations of the APD, the mode 4 required higher optical power, at least 200 pW to achieve error rates below 10^{-5}.

This level of performance yielded a margin in the power compared to the expected power levels and both mode 4 and mode 5 were tested to detect and decode the light from the moon. A stable error free Mode 5 (40 Mbits/s) down link was first demonstrated on 3/4/2014 for an operation lasting over 9 minutes. A Mode 4 down link (80 Mbits/s) was demonstrated later the same day. The Fig. 8 shows the average power level at the detector and the decoded frame error rate as a function of time. As can be seen, a stable error free operation is obtained for average power levels above 200 pW, in agreement with the characterisation using the stable laboratory source. The loss of connection in this mode for low power levels indicates that the current detector could not be used in a faster mode, i.e. Mode 3 and higher.

The present data should be compared with the results obtained by NASA using super-conducting nanowire single photon detectors (SNSPD), developed by the Lincoln lab at MIT. The SNSPD detectors are cooled down to 2 K and had been specifically optimised for the LLCD experiment. Error free down-link connexion was demonstrated even in mode 1 (625 Mbits/s) for average signal levels down to 2 photons per pulse [25]. To concurrence this performance one need to improve the sensitive and the bandwidth of the HgCdTe APD detectors. Our measurements [12] have shown that 10 GHz BW should be achieved with HgCdTe APDs detectors and the sensitivity can be increased by the hybridization of the APD on a CMOS circuit. These perspectives show that HgCdTE APDs detectors are strong candidates for space and ground based Gbit/s FSO. One possible approach for this optimization is described in the next sub-section.
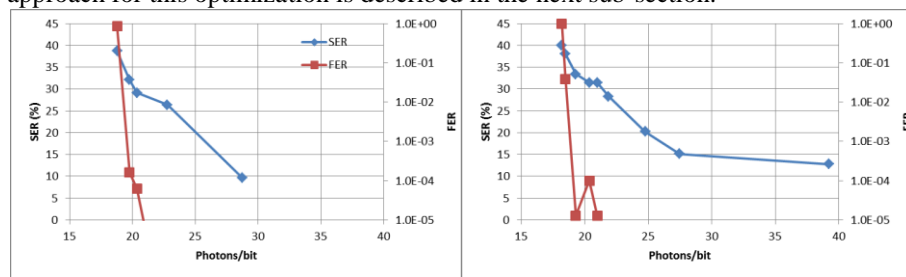

Fig. 7. Symbole error rate (SER) and fram error rate (FER) after error correction measured in) mode 5 and b) mode 4.
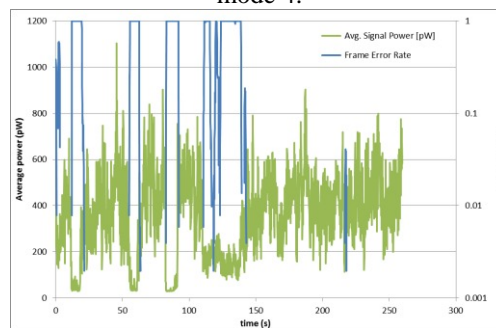

Fig. 8. Average optical power and FER detected measured with mode 4 signal from the moon on 4/4/2014.

C. Perspectives for time resolved high sensitivity detection using HgCdTe APDs for space application

The use of a deported preamplifier used for the large area single element detectors described above is a versatile solution that can be adapted to various applications requirements in terms of detector area, bandwidth and operating temperature. However, to achieve the highest sensitivity, it is mandatory to hybridize the detector onto a read-out circuit. In this case, the read-out noise can be limited to less than 100 electrons rms, without APD gain, and to values below 1 electron for high APD gains. Hence, single photon resolution can be achieved with HgCdTe APDs in this configuration, presenting a number of interesting properties for photon-counting applications such as high photon detection efficiency (PDE), absence of after-pulsing (yielding high count rates), photon number resolution (PNR) and single photon detection capability into the MWIR range.

These properties have to a large extension been confirmed by the first demonstrations of single photon detection with HgCdTe APD reported by DRS [26] and CEA/Leti [27], in particular concerning the high PDE and PNR capability. The Fig. 9 illustrates derived signals captured with the CEA/LETI HgCdTe single photon detector with a CMOS circuit limited bandwidth of 7 MHz associated with a low read-out noise of 20 electrons rms [27]. The latter allows counting photons already at low values of APD gain, which is in favor of low dark count rates. The detector used to capture the data in fig 9 was made with a MWIR APD and was consequently sensitive to residual thermal flux. The signal in Fig. 9 a) is due to the detection of such residual thermal photons

which were detected even though a cold filter was used to filter photons with $\lambda > 2.5$ µm. The Fig. 9 b) reports the signal from the same detector at zero flux. The residual events are mainly due to dark count events generated vie thermal generation in the APD. The apparent difference in amplitude between the impulses in Fig. 9 a) and b) is due to a difference in gain between photon initiated events, which are completely amplified in the APD, and thermal events in generated in the multiplication layer, for which the gain depends on the position of generation. The difference in the amplitude distribution of photon event and dark event allows to some extent filter the dark counts while obtaining a good PDE. We found that an internal PDE of 90 % could be obtained with a good filtering of the dark counts. The dark count rate (DCR) in MWIR APD has been measured to be around 200 kHz. The DCR is expected to decrease exponentially at lower λ_c, but this measurement has not yet been performed. DCR rates in order of 1 kHz are expected at an operating temperature of 80 K in such devices.
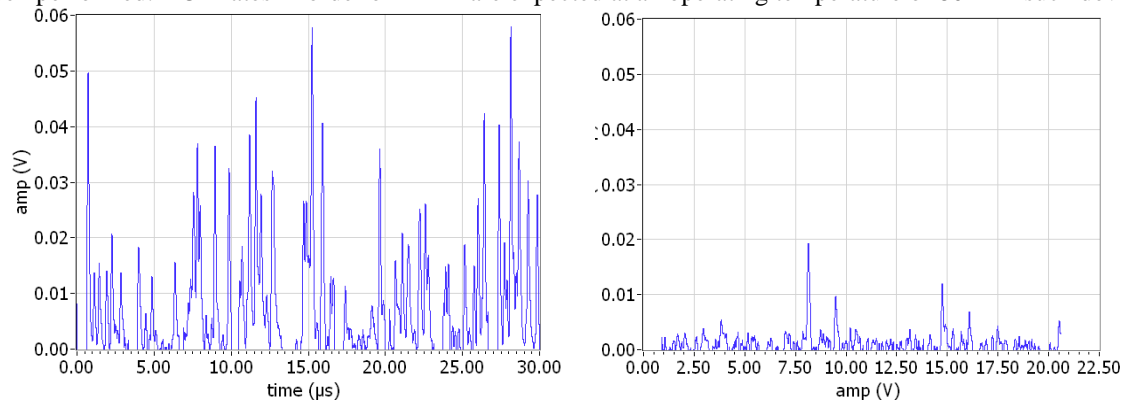
Fig 9. Output signal as a function of time with a MWIR HgCdTe APD h measured with a) a low thermal flux of photons and b) at zero flux.

The most recent development of the next generation of single photon MCT detectors has been dedicated to direct LIDAR detection of gazes such as CO2, for which single photon detection is required when the gaz concentration is measured over a large distance[28, 29]. The development of an IR photon counting LIDAR detector at LETI have been dedicated to the development of a read-out circuit which have not yet been hybridized with an APD array[28]. The detector is based on a small array of 5x5 pixels with a 30 µm pitch, in which each pixel is hybridized with an individual APD. The detector can be switched between an asynchronous photon counting mode, in which each pixel detect single photon events, and a linear mode, in which the output current of all APDs are amplified with a transimpedance amplifier. The photon counting to linear mode operation enables photon noise limited detection over more than 7 decades of input power, without modifying the APD gain.

The next priority of HgCdTe photon counting detectors will be the increase of the bandwidth of the CMOS amplifier circuit. The aim is to reach single photon sensitivity with a GHz bandwidth. A multi-pixel version of such a detector is a strong candidate for improving the sensitivity and bandwidth in deep-space FSO applications, with the potential to reach higher performance than in SNSPD combined with space compatibility in terms of operating temperature, weight and volume.

V. SUMMARY

The performance of HgCdTe APDs detectors manufactured at CEA-Leti and Sofradir . These devices have mainly been developed for active and passive photon starved imagery applications and the functionalities and the performance of the APD FPAs have been reported. Two FPA applications seems to be of main interest at present, 3D imaging for space vehicle landing and passive imaiging with sub electron noise for integration times up to 10 secondes.

Recently, we have also developed large area TEC cooled HgCdTe single element detectors. Two detector modules for atmospheric LIDAR, with low 20 MHz bandwidth and high transimpedance gain, and for FSO and laser range gating, with up to 400 MHz bandwidth and lower TIA gain. The detectors have been developed using a common packaging for low TEC cooled operation at $T < 200$ K. The measured detector modules performance are the highest that have been reported so far for high operating temperature large area linear detectors with BW > 10 MHz and characterised by NEPs between 30-70 fW/$\sqrt{\text{Hz}}$ and detector gains between 3 to 23 MV/W for detectors with 160-200 µm diameters. The faster detector module has been used to decode 80 MBits/s data from the moon with less than 50 photons per impulse. The ultimate photon counting sensitive sensitivity can be achieved when the APDs are hybridized onto a read-out circuit. Such approach is of strong interest both for the most demanding LIDAR and FSO applications.

ACKNOWLEDGEMENT

REFERENCES

[1]   J.D. Beck, C.-F. Wan, M.A. Kinch, J.E. Robinson, Proc. SPIE, 4454, 188 (2001)
[2]   J.D. Beck, C.-F. Wan, M.A. Kinch, J.E. Robinson, P. Mitra, R. Scrithfield, F. Ma, J. Campbell, J. Electron. Mater., 35,1166 (2006)
[3]   I. Baker, S. Duncan and J. Copley, Proc. SPIE, 5406, 113 (2004)
[4]   G.Perrais, O. Gravrand, J. Baylet, G.L Destefanis, J. Rothman, J. Electron. Mater., 36, 963 (2007)
[5]   M. B. Reine, J. W. Marciniec, K. K. Wong, T. Parodos, J. D. Mullarkey, P. A. Lamarre, S. P. Tobin and K. A. Gustavsen, J. Electron. Mater., 36, 1059 (2007)
[6]   J. Asbrock, S. Bailey, D Baley, J. Boisvert, G. Chapman,G. Crawford, T. De Lyon, B. Drafahl, J. Edwards, E. Herrin, C. Hoyt, M. Jack, R.Kvaas, K. Liu, W. McKeag, R. Rajavel, V. Randall, S. Rengarajan and J.Riker., Proc. SPIE, 6940, 69402O (2008)
[7]   J. Beck, M. Woodall, R. Scritchfield, M. Ohlson, L. Wood, P. Mitra, and J. Robinson, J. Electron. Mater., 37, 1334 (2008)
[8]   J. Rothman, E. de Borniol, S. Bisotto, L. Mollard, F. Guellec, F. Pistone, S. Courtas, X. Lefoule, Proc. Quantum of Quasars 2009, Pos QQ-009 (2010)
[9]   G. Perrais, J. Rothman, G. Destefanis, J-P. Chamonal, J. Electron. Mater., 37, 1261 (2008)
[10]   G. Perrais, S. Derelle, L. Mollard, J.-P. Chamonal, G. Destefanis, G. Vincent, S. Bernhardt and J. Rothman , J. Electron. Mater., 38, 1790 (2009)
[11]   R.B. Emmons, J. Appl. Phys, 38, 3705, (1967)
[12]   J. Rothman, et al., J. Electrons Mater., 43, 2947 (2014)
[13]   A. Ashcroft, I. Baker, Proc. SPIE, 7660, 76603C (2010)
[14]   I. Baker, C. Maxey, L. Hipwood, H. Weller, P. Thorne, Proc. SPIE, 8542, 85421A (2012)
[15]   J. Rothman, E. De Borniol, O. Gravrand, S. Bisotto, L. Mollard, F. Guellec, F. Pistone, S. Courtas, and X. Lefoule, Proc. SPIE 7834 78340O (2010)
[16]   E. De Borniol, P. Castelein, F. Guellec, J. Rothman, G. Vojetta, G. Destéfanis, M. Vuillermet, Proc. SPIE, 8012, 8012321 (2011)
[17]   A. Kerlain, et al., J. Electron. Mater., 41,2943, (2012)
[18]   P. Feautrier, et al., Proc. SPIE, 8447, 84470Q (2013)
[19]   E. de Borniol, et al., Proc. ICSO 2104, (2014)
[20]   O. Gravrand, et al., Proc. ICSO 2104, (2014)
[21]   K. Foubert; G. Lasfargues; L. Mathieu; S. Benahmed; G. Vojetta; J. Rothman; Q. Benoît à la Guillaume; Vincent Calvo; Jérémy Picot-Clemente; Florent Le Mounier; Fabien Gibert, Proc. SPIE, 8621, 86210F (2013)
[22]   J. Rothman, et. al, J. Electron. Mater., 41, 2928 (2012)
[23]   http://www.analogmodules.com/products/
[24]   F. Arnold, M. Mosberger, J. Widmer, F. Gambarara, , Proc. SPIE, 8971, 89710M (2014)
[25]   D. M. Boroson, et al., Proc. SPIE, 8971, 89710S (2014)
[26]   J. D. Beck ; R. Scritchfield ; P. Mitra ; W. Sullivan III ; A. D. Gleckler ; R. Strittmatter ; R. J. Martin, Proc. SPIE, 8033, 80330N (2011)
[27]   G. Vojetta, F. Guellec, L. Mathieu, K. Foubert, P. Feautrier, J. Rothman, Proc. SPIE, 8375, 83750Y (2012)
[28]   Amhaz, H. ; CEA, LETI, Grenoble, France ; Foubert, K. ; Guellec, F. ; Rothman, J., Proc. NEWCAS, (2013)
[29]   J. Beck, M. Kinch, X. Sun, Opt. Eng., 53, 81906 (2014)